Energy Efficient M -ary Frequency-Shift Keying based Modulation Techniques for Visible Light Communication

Ali Waqar Azim, Antoine Rullier, Yannis Le Guennec, Laurent Ros, Ghislaine Maury

Energy Efficient M-ary Frequency-Shift Keying based Modulation Techniques for Visible Light Communication

Ali Waqar Azim, Antoine Rullier, Yannis Le Guennec, Laurent Ros, and Ghislaine Maury

***Abstract*—In this article, we introduce two variants of energy efficient M-ary frequency-shift keying (FSK) for low data rate/low power Internet-of-Things (IoT) applications. Both variants, i.e., M-ary direct current (DC)-FSK and M-ary unipolar (U)-FSK are compatible with intensity-modulation and direct detection (IM-DD) implementation of visible light communication (VLC). The two techniques intrinsically differ in the manner of attaining a non-negative signal for intensity-modulation. M-ary DC-FSK uses a DC-offset, while, M-ary U-FSK sequentially transmits the positive and the sign flipped negative halves of the bipolar M-ary FSK symbols. The spectral efficiencies of M-ary DC-FSK and M-ary U-FSK are augmented by biorthogonal extension of frequency waveforms resulting in $2M$-ary biDC-FSK and $2M$-ary biU-FSK, respectively. Two optimal maximum likelihood (ML) receiver configurations with different complexities are introduced for M-ary DC-FSK/$2M$-ary biDC-FSK. Whereas, for M-ary U-FSK/$2M$-ary biU-FSK, an optimal ML and a sub-optimal receiver are proposed. We appraise the performance of these methods in terms of Euclidean distance, bit error rate (BER) in additive white Gaussain noise and time dispersive channels, energy efficiency with respect to spectral efficiency and computational complexity. Simulations confirm that the proposed techniques are more energy efficient than classical M-ary pulse-amplitude modulation (PAM) in an absolute sense.**

***Index Terms*—Intensity modulation and direct-detection, Internet-of-Things, visible light communication, energy efficiency, frequency-shift keying (FSK).**

I. Introduction

INTERNET-of-Things (IoT) expects ubiquitous wireless connectivity for a wide range of devices to data hosting platforms via the internet. IoT devices traditionally use radio-frequency (RF) systems to communicate. Nonetheless, pervasive connectivity of connected objects demands considerable bandwidth, which is a scarce resource. Henceforth, to relieve the dwindling RF spectrum, visible light communication (VLC) is seen as a possible complementary technology. VLC has some compelling advantages, such as license free virtually unlimited bandwidth, low-cost, high-security, no RF interference, green communication with low carbon dioxide (CO_2) footprint, concurrent communication and illumination functionalities [1]. Furthermore, omnipresence of low-cost light-emitting diode (LED) lighting infrastructures allows a cheap and non-invasive upgrade for IoT connectivity.

For VLC IoT networks, the endpoints are expected to be battery-powered LEDs based devices [2]. Thus, energy efficient communication protocols capable of operating at low sensitivity levels for inter-device networking in IoT are indispensable. To this effect, IoT networks based on VLC require diligence in designing intensity-modulation with direct-detection (IM-DD) techniques; as high energy efficiency is required to prolong the device battery lifetime [3]. Hereby, we restrict our discussion to two types of modulation categories that VLC networks may use. These categories are (i) linear modulations; and (ii) orthogonal modulations. Linear modulations include on-off keying (OOK) and M-ary pulse-amplitude modulation (PAM). These techniques are straightforward to implement and have been thoroughly investigated in the literature [4], [5], [6], [7]. OOK maintains a spectral efficiency of 1 bit/s/Hz, while the spectral efficiency of M-ary PAM, i.e., $\log_2(M)$ can be modified by changing the alphabet cardinality, M [8]. Nevertheless, for M-ary PAM, increasing the alphabet cardinality increases the required signal-to-noise ratio (SNR) per bit to reach a target bit error rate (BER). Thereupon, it is impossible for M-ary PAM to reach ultimate information theory lower-bound, i.e., Shannon's limit [9]. This also limits the usefulness of linear modulations for IoT VLC as lowest sensitivities for battery-limited endpoints cannot be attained. On the other hand, orthogonal modulations which may include M-ary pulse-position modulation (PPM) and M-ary frequency-shift keying (FSK) [10] are capable of approaching Shannon's limit by sacrificing the spectral efficiency. For orthogonal modulations, increasing alphabet cardinality, M increases the energy efficiency at an expense of relinquishing the spectral efficiency, i.e., $\log_2(M)/M$ [11], [12]. Among the orthogonal modulations, M-ary PPM has been widely studied for VLC [13]. However, it exhibits a high crest factor, high peak-to-mean optical power ratio (PMOPR) (defined in [14]) and is very sensitive to multipath propagation. This results in complex equalization and possible synchronization issues at the receiver [15], [16], [17]. M-ary FSK, on the other hand, circumvents the limitations of M-ary PPM. In this regard, [11], [12] investigate M-ary FSK as a probable substitute for low-power wide area network (LPWAN) for RF systems. Unfortunately, M-ary FSK, in its original definition, is not compatible with VLC because of its bipolar nature [10]. Yamga *et al.* [18] studied asymmetric FSK (AFSK) for VLC which uses two rectified frequency tones (two symbols) chosen depending on the transmit bit sequence. AFSK exhibits the same spectral efficiency as OOK and does not provide any gain in sensitivity. As shall become apparent in the sequel, our proposed techniques use a large set of symbols with different frequencies rather than using two frequency tones as in AFSK.

To the best of our knowledge, this paper is the first one to intrinsically amalgamate M-ary FSK with VLC for IoT.

Ali Waqar Azim, Antoine Rullier, Yannis Le Guennec and Laurent Ros are with Université Grenoble Alpes, CNRS, Institute of Engineering, Grenoble INP, GIPSA-LAB, 38000 Grenoble, France (email: {ali-waqar.azim, yannis.leguennec, laurent.ros}@gipsa-lab.grenoble-inp.fr, antoine.rullier@isae-alumni.net). Ghislaine Maury is with Université Grenoble Alpes, CNRS, Institute of Engineering, Grenoble INP, IMEP-LAHC, 38000 Grenoble, France (email: maury@grenoble-inp.fr).

We propose two VLC compatible M-ary FSK variants: M-ary direct-current (DC)-FSK and M-ary unipolar (U)-FSK. Biorthogonal extention of these approaches leads to $2M$-ary biDC-FSK and $2M$-ary biU-FSK, respectively. For M-ary DC-FSK and $2M$-ary biDC-FSK, two optimal maximum likelihood (ML) receiver configurations with different complexities but same BER performances are presented. On the other hand, for M-ary U-FSK and $2M$-ary biU-FSK, high-complexity optimal ML and low-complexity sub-optimal receivers are introduced. It may also be noticed that the proposed low-complexity receiver configurations are applicable to fast-orthogonal frequency-division multiplexing (FOFDM) approaches in [19] with no modification. This may further enhances the verstality of the our proposed techniques.

A. Notations

Lower-case boldface italic letters denote discrete time-domain vectors, e.g., $\boldsymbol{s}_m$, where m in the subscript identifies the activated frequency tone. The analog signal is denoted as $s_m(t)$. Lower-case italic letters with an index, e.g., $s_m[n]$ represent the nth element of the discrete time-domain vector, $\boldsymbol{s}_m$. Discrete cosine transform (DCT) of discrete time-domain vector, e.g., $\boldsymbol{r}$ is given by upper-case boldface italic letters, e.g., $\boldsymbol{R}$. Boldface calligraphic letters, e.g., $\boldsymbol{\mathcal{D}}$ are used for matrices. $|\cdot|$, $\|\cdot\|$ $(\cdot)^{\mathrm{T}}$, $\langle\cdot,\cdot\rangle$ and $\otimes$ respectively represent absolute, Euclidean norm, transpose, inner product and convolution operators.

B. Paper Organization

The rest of the article is organized as follows. FSK generation, correlation properties, system model and the motivations are presented in Section II. Section III presents the proposed approaches and an analytical analysis of Euclidean distance. Spectral efficiencies and complexities are also discussed in Section III. Section IV elucidates the improved receiver design for time dispersive channels. The performances of the proposed approaches over additive white Gaussian noise (AWGN) and optical time dispersive channels by numerical simulations are discussed in Section V. Based on simulation results, conclusions are rendered in Section VI.

II. Preliminaries

A. Conventional and Biorthogonal FSK Generation

Conventional M-ary FSK specifies a dictionary, $\boldsymbol{\mathcal{D}}_{\perp}$, of M orthogonal sinusoidal waveforms, with the frequency of each waveform identified via an index, $\tilde{m} \in \{0, 1, \cdots, M-1\}$. The digital time series waveform corresponding to $\tilde{m}$th frequency, $\tilde{\boldsymbol{s}}_{\tilde{m}} = [\tilde{s}_{\tilde{m}}[0], \tilde{s}_{\tilde{m}}[1], \cdots, \tilde{s}_{\tilde{m}}[M-1]]^{\mathrm{T}}$, is obtained as [20]:

$$\tilde{\boldsymbol{s}}_{\tilde{m}} = \boldsymbol{\mathcal{C}}^{\mathrm{T}} \boldsymbol{S}_{\tilde{m}}, \tag{1}$$

with $\boldsymbol{S}_{\tilde{m}} = [0, \cdots, 1, \cdots, 0]^{\mathrm{T}}$. The non-zero index of $\boldsymbol{S}_{\tilde{m}}$ determines the frequency tone, e.g., $S_{\tilde{m}} = 1$ at $\tilde{m}$th index implies that $\tilde{m}$th frequency is active. $\boldsymbol{\mathcal{C}}$ is the DCT matrix whose (n_1, n_2)th element is [21]:

$$\mathcal{C}_{n_1,n_2} = \begin{cases} \frac{1}{\sqrt{M}} & n_1 = 0 \\ \sqrt{\frac{2}{M}} \cos\left(\frac{\pi(2n_2+1)n_1}{2M}\right) & 1 \leq n_1 \leq M-1 \end{cases}, \tag{2}$$

where $0 \leq n_2 \leq M-1$. We use DCT to generate the frequency waveforms instead of discrete Fourier transform (DFT) because it is a real transform which does not require Hermitian symmetry to attain real-valued output.

We consider a chip period (sample period) of T_{c} and a symbol duration of $T_{\mathrm{s}} = M_{\mathrm{c}} T_{\mathrm{c}}$, where M_{c} is the number of chips per symbol. For conventional (bipolar) M-ary FSK, $M_{\mathrm{c}} = M$, and the symbol duration is $T_{\mathrm{s}} = \tilde{T}_{\mathrm{s}}$ with $\tilde{T}_{\mathrm{s}} = MT_{\mathrm{c}}$. The orthogonality condition for any two pairs of symbol in discrete-time domain is given as [11]:

$$\langle \tilde{s}_i[n], \tilde{s}_j[n] \rangle = \sum_{n=0}^{M_{\mathrm{c}}-1} \tilde{s}_i[n] \tilde{s}_j[n] = \begin{cases} 0 & \text{for } i \neq j \\ 1 & \text{for } i = j \end{cases}, \tag{3}$$

for $(i, j) \in \{0, 1, \cdots, M-1\}^2$. The analog counterpart of $\tilde{s}_{\tilde{m}}[n]$, i.e., $\tilde{s}_{\tilde{m}}(t)$ is obtained using $t = \left(n + \frac{1}{2}\right) T_{\mathrm{c}}$ as:

$$\tilde{s}_{\tilde{m}}(t) = \begin{cases} \frac{A}{\sqrt{2}} & \tilde{m} = 0 \\ A \cos\left(2\pi \tilde{m} \Delta f t\right) & 1 \leq \tilde{m} \leq M-1 \end{cases}, \tag{4}$$

where A is the waveform amplitude and $\Delta f = 1/2\tilde{T}_{\mathrm{s}}$ is the frequency spacing between adjacent waveforms. Note that, $\tilde{s}_{\tilde{m}}(t)$ are also orthogonal in analog domain, i.e.,

$$\langle \tilde{s}_i(t), \tilde{s}_j(t) \rangle = \begin{cases} 0 & i \neq j \\ \frac{A^2}{2} \tilde{T}_{\mathrm{s}} = E_{\mathrm{s}}^{\mathrm{FSK}} & i = j \end{cases}, \tag{5}$$

where $E_{\mathrm{s}}^{\mathrm{FSK}}$ is the average (electrical) symbol energy of M-ary FSK.

As $\tilde{\boldsymbol{s}}_{\tilde{m}}$ is bipolar, some modifications are required to define IM-DD compatible M-ary FSK modulations. These modifications to attain non-negativity of the transmit siganl shall become apparent in the subsequent subsections. For implementation, a pragmatic way to assemble all the waveforms is to interpolate them in a look-up-table (LUT); from which, the chosen waveform can be directly extrapolated, thus, reducing the overall system complexity.

(1) and (4) establish the possibility of extending the cardinality of dictionary, $\boldsymbol{\mathcal{D}}_{\perp}$, from M to $2M$ waveforms by defining a biorthogonal dictionary, $\boldsymbol{\mathcal{D}}_{\mathrm{b}}$; which includes the negatives of original waveforms. By doing so, the spectral efficiency can be increased. For clarity of notation, the waveforms are given by $\tilde{s}_m(t)$ in contrast to $\tilde{s}_{\tilde{m}}(t)$ for $\boldsymbol{\mathcal{D}}_{\perp}$ and are indexed by m, where $m \in \{0, 1, \cdots, 2M-1\}$. The waveforms corresponding to $M \leq m \leq 2M-1$ in $\boldsymbol{\mathcal{D}}_{\mathrm{b}}$ are negative versions of the waveforms with indices $0 \leq m \leq M-1$ in $\boldsymbol{\mathcal{D}}_{\perp}$, i.e., $\boldsymbol{\mathcal{D}}_{\mathrm{b}} = \{\boldsymbol{\mathcal{D}}_{\perp}; -\boldsymbol{\mathcal{D}}_{\perp}\}$. Hence, (4) is valid for $\tilde{s}_m(t)$ if $0 \leq m \leq M-1$ and

$$\tilde{s}_m(t) = -\tilde{s}_{m-M}(t), \tag{6}$$

if $M \leq m \leq 2M-1$. To elaborate, the phase applied to the second subset of sinusoids is π instead of 0 as for the first subset. The resulting squared Euclidean distance, $\tilde{d}_{i,j}^2$, for any

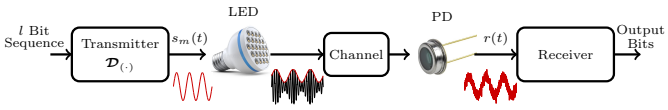

Fig. 1: Generalized system model.

two pairs of different waveforms is

$$\tilde{d}_{i,j}^2 = \|\tilde{s}_i(t) - \tilde{s}_j(t)\|^2 = \begin{cases} 2E_{\mathrm{s}}^{\mathrm{FSK}} & |j-i| \neq 0, M \\ 4E_{\mathrm{s}}^{\mathrm{FSK}} & |j-i| = M \end{cases}, \quad (7)$$

for $(i,j) \in \{0,1,\cdots,2M-1\}^2$. Thus, the minimum squared Euclidean distance of the dictionary, $\boldsymbol{\mathcal{D}}_{\mathrm{b}}$ is $d_{\min}^2 = \min_{i \neq j} \tilde{d}_{i,j}^2 = 2E_{\mathrm{s}}^{\mathrm{FSK}}$. It is highlighted that the minimum squared Euclidean distance for $\boldsymbol{\mathcal{D}}_{\mathrm{b}}$ is the same as that of $\boldsymbol{\mathcal{D}}_{\perp}$ for M-ary FSK.

B. System Model

Consider the system configuration in Fig. 1. A generalized dictionary of cardinality $|\boldsymbol{\mathcal{D}}_{(\cdot)}|$ is considered, where $(\cdot)$ in the subscript refers to both orthogonal and biorthogonal dictionaries. The intensity waveform with mth activated tone, $s_m(t)$, modulates the luminance of the LED. The time series representation of $s_m(t)$ is $s_m[n]$ for $0 \leq n \leq M_{\mathrm{c}} - 1$. The index (frequency) of the waveform, m, is determined via binary to decimal mapping of $l = \log_2(|\boldsymbol{\mathcal{D}}_{(\cdot)}|)$ independent and equiprobable bits. For disambiguation, the sampled version, $s_m[n]$ is called *symbol*; which in vectorial form is expressed as $\boldsymbol{s}_m = [s_m[0], s_m[1], \cdots, s_m[M_{\mathrm{c}}-1]]^{\mathrm{T}}$. Each symbol is a sequence of $T_{\mathrm{s}}/T_{\mathrm{c}} = M_{\mathrm{c}}$ chips with a bit rate, R_{b} of $\log_2(|\boldsymbol{\mathcal{D}}_{(\cdot)}|)/T_{\mathrm{s}}$[1]. $s_m(t)$ is transformed into an optical intensity waveform $u_m(t) = \varepsilon s_m(t)$, with ε Watt (W)/Ampere (A) being the electrical-to-optical conversion factor. Perfect synchronization is considered at the receiver [22], [23]. The impulse response of the channel is given by $h(t)$. The photo-detected waveform is $g_m(t) = \kappa\,(h(t) \otimes u_m(t))$, where κ A/W is the responsitivity of the photo-diode (PD). Moreover, following [24], a linear response for the LED and PD is adopted. Without loss of generality, we consider $\varepsilon = 1$ W/A and $\kappa = 1$ A/W, hence, $g_m(t) = h(t) \otimes u_m(t)$ and $u_m(t) = s_m(t)$. The received waveform is contaminated by the ambient noise resulting in $r(t)$. After impinging $r(t)$ on an analog-to-digital converter (ADC), we obtain:

$$\boldsymbol{r} = \boldsymbol{h} \otimes \boldsymbol{s}_m + \boldsymbol{w}, \quad (8)$$

where $\boldsymbol{w}$ is AWGN with mono-lateral power spectral density (PSD) of N_0. Explicitly, $\boldsymbol{r} = [r[0], r[1], \cdots, r[M_{\mathrm{c}}-1]]^{\mathrm{T}}$, $\boldsymbol{w} = [w[0], w[1], \cdots, w[M_{\mathrm{c}}-1]]^{\mathrm{T}}$, and $\boldsymbol{h} = [h[0], h[1], \cdots, h[M_{\mathrm{c}}-1]]^{\mathrm{T}}$. For simplicity, till the end of Section III, we shall consider an AWGN channel whose impulse response is $h(t) = \delta(t)$, where $\delta(t)$ represents the Dirac distribution.

For brevity, we shall only present the techniques based on extended dictionary, i.e., $\boldsymbol{\mathcal{D}}_{\mathrm{b}}$, leading in Section III to consider $2M$-ary biDC-FSK and $2M$-ary biU-FSK. Moreover, these techniques are investigated considering single user. Multiple users scenarios can be adequately addressed using physical layer multiple access protocols, such as time-division multiple access (TDMA), frequency-division multiple access (FDMA) [25], [26]. However, an investigation into the applicability of multiple access is beyond the purview of this article.

[1]We use the notation, T_{s} to specify the symbol time for the proposed approaches. In the sequel, T_{s} would be defined in terms of the symbol duration of conventional M-ary FSK, i.e., $\tilde{T}_{\mathrm{s}} = MT_{\mathrm{c}}$.

C. Motivations

The goal is to develop energy efficient VLC compatible modulations which can be used for low data rate/low power IoT applications. Thereby, to formulate a framework, we consider the average electrical power of the transmit symbol, $P_{(\mathrm{elec})} = E_{\mathrm{s}_{(\mathrm{elec})}}/T_{\mathrm{s}} = E_{\mathrm{b}_{(\mathrm{elec})}} R_{\mathrm{b}}$, where $E_{\mathrm{s}_{(\mathrm{elec})}}$ is the average electrical energy per symbol and $E_{\mathrm{b}_{(\mathrm{elec})}}$ is the average electrical energy per bit. In AWGN channel, without considering any interference from other users (single user scenario), the electrical SNR of the system, $\mathrm{SNR}_{(\mathrm{elec})}$ is

$$\mathrm{SNR}_{(\mathrm{elec})} \triangleq \frac{P_{(\mathrm{elec})}}{\sigma_n^2} = \frac{E_{\mathrm{b}_{(\mathrm{elec})}}}{N_0}\eta, \quad (9)$$

where $\sigma_n^2 = N_0 B$ is the noise variance, $\eta = R_{\mathrm{b}}/B$ is the spectral efficiency in bit/s/Hz, and $B = 1/2T_{\mathrm{c}}$ is the mono-lateral communication bandwidth in Hz. Shannon's limit [9] bounds the spectral efficiency, η in (9). In fact, it gives an upper bound on the attainable data rate for an arbitrarily low BER for a given $\mathrm{SNR}_{(\mathrm{elec})}$ and bandwidth, B in an AWGN channel. Notably, the Shannon's fundamental limit can only be achieved using a bipolar signal, which is not the case with IM-DD. However, without loss of generality, it can be used as a pessimistic lower bound for the unipolar signal. According to Shannon's theorem, the data rate is limited by [10]:

$$R_{\mathrm{b}} \leq B \log_2\left(1 + \mathrm{SNR}_{(\mathrm{elec})}\right) \quad \text{(bit/s)}. \quad (10)$$

Normalizing (10) by the bandwidth, B and taking into account (9), the bound on spectral efficiency, η is obtained as [11], [12]:

$$\eta \leq \log_2\left(1 + \frac{E_{\mathrm{b}_{(\mathrm{elec})}}}{N_0}\eta\right). \quad (11)$$

Reformulating (11) in terms of minimum required average electrical energy per bit, $(E_{\mathrm{b}_{(\mathrm{elec})}}/N_0)_{\min}$ for a given spectral efficiency, η, we get [11], [12]

$$\frac{E_{\mathrm{b}_{(\mathrm{elec})}}}{N_0} \geq \frac{2^\eta - 1}{\eta} = \left(\frac{E_{\mathrm{b}_{(\mathrm{elec})}}}{N_0}\right)_{\min}. \quad (12)$$

(12) implies that $\left(E_{\mathrm{b}_{(\mathrm{elec})}}/N_0\right)_{\min}$ is an increasing function of the spectral efficiency, η. Conventionally, for a bipolar signal, the asymptotic limit on $\left(E_{\mathrm{b}_{(\mathrm{elec})}}/N_0\right)_{\min}$, i.e., Shannon's fundamental limit is attained when $\eta \to 0$ resulting in $(E_{\mathrm{b}_{(\mathrm{elec})}}/N_0)_{\mathrm{lim}} = \ln(2) \simeq -1.59$ dB. This signifies a compromise between the achievable spectral efficiency and the energy efficiency.

For orthogonal modulations, considering bandwidth B, symbol duration, T_{s}, and assuming $B \gg 1/T_{\mathrm{s}}$, a set of $M = 2BT_{\mathrm{s}}$ orthogonal waveforms can be defined. For a given $E_{\mathrm{b}_{(\mathrm{elec})}}/N_0$, if M increases, the minimum squared distance between the symbols, i.e., $d_{\min}^2 = 2E_{\mathrm{s}_{(\mathrm{elec})}} = 2E_{\mathrm{b}_{(\mathrm{elec})}} \log_2(M)$ also increases. Hence, the required $E_{\mathrm{b}_{(\mathrm{elec})}}/N_0$ for reliable

communication tends toward the lower bound of -1.59 dB as M goes to infinity. We recall that this behavior is in complete contradiction to the linear modulations, where the minimum distance diminishes with an increase in modulation alphabet cardinality resulting in an increase of required $E_{\mathrm{b}_{(\mathrm{elec})}}/N_0$ for a given BER [27].

For both RF and IM-DD systems, in addition to dispersive channel sensitivity and receiver synchronization issues, M-ary PPM exhibits a factor M dependency for peak-to-average-power ratio (PAPR) and PMOPR which induces strong limitations with realistic amplitude limited transmitters, especially when targetting high energy efficiency (i.e., large M value) for IoT applications. On the other hand, for M-ary FSK, the limitations are of different nature. Regardless of the fact that it manifests constant envelope property and easy channel equalization [11], [27], the transmit signal is bipolar; which cannot be transmitted using LED because of the required positive bias current. Motivated by the state-of-the-art, we propose and evaluate the performances of the variants of M-ary FSK compatible with VLC, which may be used for low data rate/low power IoT applications.

III. Proposed Approaches and Analysis

To exploit the benefits of M-ary FSK, we introduce $2M$-ary biDC-FSK in subsection III-A and $2M$-ary biU-FSK in subsection III-B. Both approaches are compatible with IM-DD VLC. Note that, in this section, the principle of the proposed approaches is presented considering an AWGN channel, i.e., $h(t) = \delta(t)$. The development of the proposed approches considering a time dispersive VLC channel shall be presented subsequently. Hereby, we also present the spectral efficiencies, distance analysis and computational complexities for the proposed approaches. The details of these techniques are outlined in the following subsections.

A. $2M$-ary biDC-FSK

1) Transmitter: We consider $2M$-ary biDC-FSK transmitter configuration shown in Fig. 2, where mth waveform is chosen by binary to decimal conversion of $l = \log_2(2M)$ independent and equiprobable bits. The symbol conforming to the chosen frequency and polarity, $\tilde{s}_m[n]$ is extrapolated from LUT. Subsequently, a DC-offset, β_{DC} is added to $\tilde{s}_m[n]$ resulting in $s_m[n]$, which defines $2M$-ary biDC-FSK dictionary, $\boldsymbol{\mathcal{D}}_{\mathrm{b}}^{\mathrm{DC}}$. In fact, $\boldsymbol{\mathcal{D}}_{\mathrm{b}}^{\mathrm{DC}} = \beta_{\mathrm{DC}} + \boldsymbol{\mathcal{D}}_{\mathrm{b}}$, where the number of chips, $M_{\mathrm{c}} = M$. As an example, illustration of $s_2[n]$ extrapolated from $\boldsymbol{\mathcal{D}}_{\mathrm{b}}^{\mathrm{DC}}$ is presented in Fig. 3. $\tilde{s}_m(t)$ is obtained by impinging $s_m[n]$ on a digital-to-analog converter (DAC) and considering $t = \left(n + \frac{1}{2}\right) T_{\mathrm{c}}$. The mth waveform for $2M$-ary biDC-FSK is given as:

$$s_m(t) = \tilde{s}_m(t) + \beta_{\mathrm{DC}}, \tag{13}$$

where $t \in [0, T_{\mathrm{s}}]$. For $2M$-ary biDC-FSK, $T_{\mathrm{s}} = \tilde{T}_{\mathrm{s}}$ and the average electrical energy per symbol is:

$$E_{\mathrm{s}_{(\mathrm{elec})}}^{\mathrm{DC}} = \frac{1}{2M} \sum_{m=0}^{2M-1} \int_0^{\tilde{T}_{\mathrm{s}}} s_m^2(t)\mathrm{d}t = \tilde{T}_s \left(\frac{A^2}{2} + \beta_{\mathrm{DC}}^2 \right). \tag{14}$$

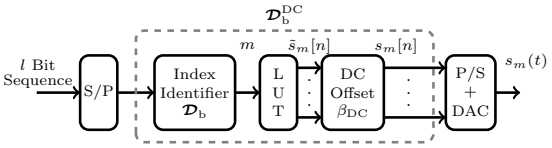

Fig. 2: Transmitter configuration for $2M$-ary biDC-FSK.

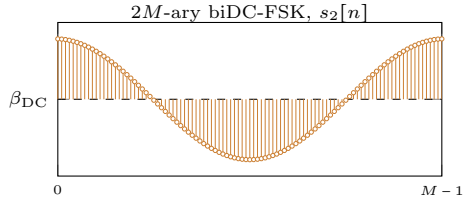

Fig. 3: An illustration of $s_2[n]$ drawn from $2M$-ary biDC-FSK's LUT.

All the waveforms have the same electrical energy, i.e., $\int_0^{\tilde{T}_{\mathrm{s}}} s_m^2(t)\mathrm{d}t = E_{\mathrm{s}_{(\mathrm{elec})}}^{\mathrm{DC}}$, except for $s_0(t)$ and $s_M(t)$, for which the electrical energy per symbols are $\int_0^{\tilde{T}_{\mathrm{s}}} s_0^2(t)\mathrm{d}t = E_{\mathrm{s}_{(\mathrm{elec})}}^{\mathrm{DC}} + \sqrt{2}A\beta_{\mathrm{DC}}$ and $\int_0^{\tilde{T}_{\mathrm{s}}} s_M^2(t)\mathrm{d}t = E_{\mathrm{s}_{(\mathrm{elec})}}^{\mathrm{DC}} - \sqrt{2}A\beta_{\mathrm{DC}}$, respectively.

Unfortunately, the addition of DC-offset affects the orthogonality between the waveforms because:

$$\langle s_i(t), s_j(t) \rangle = \int_0^{\tilde{T}_{\mathrm{s}}} s_i(t) s_j(t)\mathrm{d}t = \beta_{\mathrm{DC}}^2 \tilde{T}_{\mathrm{s}} \quad \forall i \neq j \neq 0. \tag{15}$$

The minimum value of the DC-offset, β_{DC} to achieve non-negative transmit signal is A, resulting in $E_{\mathrm{s}_{(\mathrm{elec})}}^{\mathrm{DC}}$ in (14) equal to $3E_{\mathrm{s}}^{\mathrm{FSK}}$. Using (7), (14) and (15) and considering $\beta_{\mathrm{DC}} = A$, the squared Euclidean distance for $2M$-ary biDC-FSK is

$$\tilde{d}_{i,j}^2 = \begin{cases} 2E_{\mathrm{s}_{(\mathrm{elec})}}^{\mathrm{DC}} \times \gamma^{\mathrm{DC}} & |j-i| \neq 0,\ M \\ 4E_{\mathrm{s}_{(\mathrm{elec})}}^{\mathrm{DC}} \times \gamma^{\mathrm{DC}} & |j-i| = M \end{cases}, \tag{16}$$

for $(i, j) \in \{0, 1, \cdots, 2M-1\}^2$, where $\gamma^{\mathrm{DC}} = 1/3$. The minimum squared Euclidean distance for $2M$-ary biDC-FSK is equal to $\min_{i \neq j} \tilde{d}_{i,j}^2$, i.e.,

$$d_{\min,\mathrm{DC}}^2 = \min_{i \neq j} \tilde{d}_{i,j}^2 = 2E_{\mathrm{s}_{(\mathrm{elec})}}^{\mathrm{DC}} \times \gamma^{\mathrm{DC}}. \tag{17}$$

For M-ary FSK, γ^{FSK} is equal to 1 (see Section II-C). Note that, $\gamma^{\mathrm{DC}} < \gamma^{\mathrm{FSK}}$ due to the addition of the DC-offset.

2) Receiver:

a) Theoretical Maximum Likelihood Receiver: The receiver structure for $2M$-ary biDC-FSK is presented in Fig. 4. At the receiver, $r[n]$ for $n = 0, 1, \cdots, M-1$ is attained post analog-to-digital conversion of the received waveform, $r(t)$. The optimal ML minimum distance receiver for $2M$-ary biDC-FSK is

$$\hat{m} = \arg\min_{m} \|\boldsymbol{r} - \boldsymbol{s}_m\|^2. \tag{18}$$

A practical way to implement (18) is to estimate and remove the DC-offset, β_{DC} from the received symbols resulting in $\tilde{\boldsymbol{r}} = \boldsymbol{r} - \beta_{\mathrm{DC}}$. The symbols, $\tilde{\boldsymbol{r}}$ are independent, equal-energy, memory-less. Hence, (18) is implemented by determining the symbol, $\tilde{\boldsymbol{s}}_m$ in $\boldsymbol{\mathcal{D}}_{\mathrm{b}}$, which provides the highest value of cross-

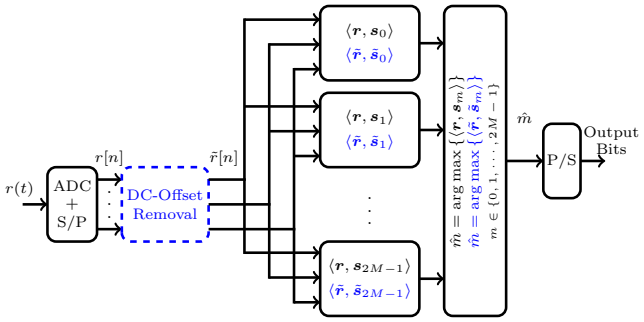

Fig. 4: Theoretical MLreceiver configuration for $2M$-ary biDC-FSK. In addition to the operations in black color, the operations performed in blue color corresponds to $2M$-ary biDC-FSK receiver. This structure also corresponds to the optimal ML receiver for $2M$-ary biU-FSK, all the operations in black corresponds to what is needed for the ML receiver of $2M$-ary biU-FSK.

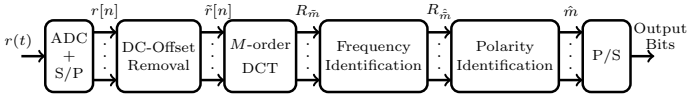

Fig. 5: Low-complexity ML receiver configuration for $2M$-ary biDC-FSK.

correlation with $\tilde{\boldsymbol{r}}$, i.e.,

$$\hat{m} = \arg\max_{m} \Big\{ \langle \tilde{\boldsymbol{r}}, \tilde{\boldsymbol{s}}_m \rangle \Big\}. \tag{19}$$

The complexity of ML receiver in (19) (Fig. 4) is of the order of $\mathcal{O}(M^2)$.

b) Low-complexity Maximum Likelihood Receiver: An alternate low-complexity but optimal receiver is illustrated in Fig. 5, where the frequencies are assembled using M-order DCT on $\tilde{\boldsymbol{r}}$ as:

$$\boldsymbol{R}_{\tilde{m}} = \boldsymbol{\mathcal{C}} \tilde{\boldsymbol{r}}, \tag{20}$$

where $\boldsymbol{R}_{\tilde{m}} = [R_0, R_1, \cdots, R_{M-1}]^{\mathrm{T}} \in \Re^M$. Using (20), the detection of the transmitted waveform frequency is made using $\tilde{m} \in \{0, 1, \cdots, M-1\}$ as:

$$\hat{\tilde{m}} = \arg\max_{\tilde{m}} \Big\{ |R_{\tilde{m}}| \Big\}. \tag{21}$$

Afterwards, the polarity of $\boldsymbol{R}_{\tilde{m}}$ at index $\hat{\tilde{m}}$ determines the index among $m \in \{0, 1, \cdots, 2M-1\}$ of the transmitted waveform as:

$$\hat{m} = \begin{cases} \hat{\tilde{m}} & \text{if } R_{\hat{\tilde{m}}} > 0 \\ \hat{\tilde{m}} + M & \text{if } R_{\hat{\tilde{m}}} < 0 \end{cases}. \tag{22}$$

The computational complexity of the receiver is discussed afterwards. Though $2M$-ary biDC-FSK fulfills the constraints of VLC, the use of DC-offset lessens the energy efficiency.

B. $2M$-ary biU-FSK

By averting the use of DC-offset, an alternative approach, $2M$-ary biU-FSK is investigated. $2M$-ary biU-FSK sequentially disseminates positive amplitude samples of M-ary FSK symbol (the negative samples are forced to zero) in a first period and polarity reversed negative amplitude samples in a following period (the positive sampled are forced to zero). Thus, the overall symbol duration T_{s} is increased by twofolds and the number of chips is doubled, i.e., $T_{\mathrm{s}} = 2\tilde{T}_{\mathrm{s}}$ and $M_{\mathrm{c}} = 2M$, respectively.

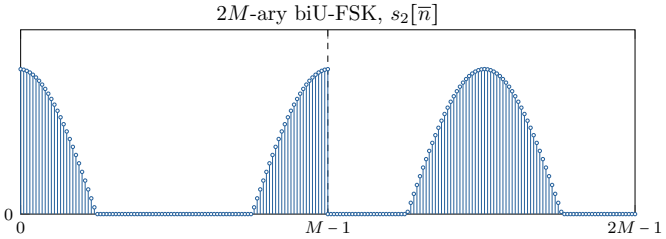

Fig. 6: An illustration of $s_2[\overline{n}]$ drawn from $2M$-ary biU-FSK's LUT.

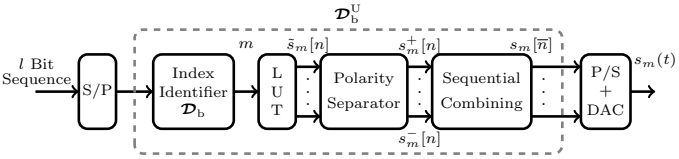

Fig. 7: Transmitter configuration for $2M$-ary biU-FSK.

1) Transmitter: We consider the $2M$-ary biU-FSK transmitter illustrated in Fig. 7. The symbol corresponding to index m, i.e., $\tilde{s}_m[n]$ is extrapolated using dictionary, $\boldsymbol{\mathcal{D}}_{\mathrm{b}}$. m is determined by binary to decimal conversion of $l = \log_2(2M)$ independent and equiprobable bits. To generate the $2M$-ary biU-FSK dictionary, $\boldsymbol{\mathcal{D}}_{\mathrm{b}}^{\mathrm{U}}$ from $\boldsymbol{\mathcal{D}}_{\mathrm{b}}$, we consider $\tilde{s}_m[n]$ as in (6). The positive and negative amplitude excursions of $\tilde{s}_m[n]$ are obtained as:

$$\tilde{s}_m^+[n] = \frac{1}{2} \left(\tilde{s}_m[n] + |\tilde{s}_m[n]| \right), \tag{23}$$

and

$$\tilde{s}_m^-[n] = \frac{1}{2} \left(\tilde{s}_m[n] - |\tilde{s}_m[n]| \right), \tag{24}$$

respectively.

Thereafter, $2M$-ary biU-FSK dictionary, $\boldsymbol{\mathcal{D}}_{\mathrm{b}}^{\mathrm{U}}$ is obtained via unipolar symbols constructed from $\tilde{s}_m^+[n]$ and $\tilde{s}_m^-[n]$ as:

$$s_m[\overline{n}] = \begin{cases} \tilde{s}_m^+[\overline{n}] & 0 \le \overline{n} \le M-1 \\ -\tilde{s}_m^-[\overline{n} - M] & M \le \overline{n} \le 2M-1 \end{cases}. \tag{25}$$

$\overline{n}$ specifies $2M$ chips of $2M$-ary biU-FSK. An example of $s_2[\overline{n}]$ extracted from $2M$-ary biU-FSK dictionary, $\boldsymbol{\mathcal{D}}_{\mathrm{b}}^{\mathrm{U}}$, is illustrated in Fig. 6. After digital to analog conversion of $s_m[\overline{n}]$ using $t = \left(\overline{n} + \frac{1}{2}\right) T_{\mathrm{c}}$ and owing to (4) and (6), the symbols in analog domain, $s_m(t)$ are expressed as:

$$s_m(t) = \begin{cases} \frac{1}{2} \left(\tilde{s}_m(t) + |\tilde{s}_m(t)| \right) & [0, \tilde{T}_{\mathrm{s}}] \\ \frac{1}{2} \left(\tilde{s}_m(t - \tilde{T}_{\mathrm{s}}) - |\tilde{s}_m(t - \tilde{T}_{\mathrm{s}})| \right) &]\tilde{T}_{\mathrm{s}}, 2\tilde{T}_{\mathrm{s}}] \end{cases}, \tag{26}$$

which are then transmitted via an LED.

It is accentuated that $2M$-ary biU-FSK waveforms have equal symbol energy, which is equal to original M-ary FSK waveform energy, i.e., $E_{\mathrm{s(elec)}}^{\mathrm{U}} = \left(A^2/2\right) \tilde{T}_{\mathrm{s}} = E_{\mathrm{s}}^{\mathrm{FSK}}$. Moreover, the minimal squared Euclidean distance between two $2M$-ary biU-FSK waveforms is computed as:

$$\begin{aligned} d_{\min,\mathrm{U}}^2 &= \min_{i \neq j} \|s_i(t) - s_j(t)\|^2 \\ &= \min_{i \neq j} \left\{ 2E_{\mathrm{s}}^{\mathrm{FSK}} - 2\langle s_i(t), s_j(t) \rangle \right\} \end{aligned} \tag{27}$$

The transformation of bipolar M-ary FSK into $2M$-ary biU-FSK impacts the orthogonality between the waveforms.

Consequently, for any pair of waveforms, $s_i(t)$ and $s_j(t)$ in the dictionary, $\boldsymbol{\mathcal{D}}_{\mathrm{b}}^{\mathrm{U}}$, the scalar products, $\langle s_i(t), s_j(t)\rangle$, are not identical. However, it is feasible to ascertain an upper bound on $\langle s_i(t), s_j(t)\rangle$, from which, a lower bound on the squared minimal Euclidean distance (27) can be achieved. We observe that the squared minimum Euclidean distance is identical for both M-ary U-FSK or $2M$-ary biU-FSK, therefore, we shall only consider $\tilde{m} \in \{0, 1, \cdots, M-1\}$ for this analysis. It has been observed that the maximum value of $\langle s_i(t), s_j(t)\rangle$ is achieved via dot product of $s_0(t)$ and $s_{\tilde{m}}(t)$, where, $\tilde{m} \neq 0$ and $1 \leq \tilde{m} \leq M-1$ resulting in:

$$\langle s_0(t), s_{\tilde{m}\neq 0}(t)\rangle = \frac{A}{\sqrt{2}} \int_0^{\tilde{T}_{\mathrm{s}}} s_{\tilde{m}\neq 0}(t)\mathrm{d}t = \frac{\sqrt{2}A^2\tilde{T}_{\mathrm{s}}}{2\pi}. \quad (28)$$

Using (28), the lower bound on (27) is evaluated to be:

$$d^2_{\min,\mathrm{U},\mathrm{lb}} = A^2\tilde{T}_{\mathrm{s}} - \frac{\sqrt{2}A^2\tilde{T}_{\mathrm{s}}}{\pi} = 2E^{\mathrm{U}}_{\mathrm{s}_{(\mathrm{elec})}} \times \gamma^{\mathrm{U}}, \quad (29)$$

where $\gamma^{\mathrm{U}} = \left(1 - \sqrt{2}/\pi\right) \approx 0.55$. Simulations reveal that the Euclidean distance between two waveforms does not exceed 4.65% of the lower bound, $d_{\min,\mathrm{U},\mathrm{lb}}$. Moreover, it is foreseen that the energy efficiency of $2M$-ary biU-FSK is better than $2M$-ary DC-FSK, since $\gamma^{\mathrm{U}} > \gamma^{\mathrm{DC}}$.

2) Receiver:

a) Theoretical Maximum Likelihood Receiver: The optimal ML receiver structure for $2M$-ary biU-FSK is the same as portrayed in Fig. 4, however, the dictionary considered is $\boldsymbol{\mathcal{D}}_{\mathrm{b}}^{\mathrm{U}}$. For the optimal ML receiver, as we have equal-energy waveforms, the transmit frequency is identified using the cross-correlation between $\boldsymbol{r}$ and $\boldsymbol{s}_m \in \boldsymbol{\mathcal{D}}_{\mathrm{b}}^{\mathrm{U}}$ as:

$$\hat{m} = \arg\max_m \Big\{ \langle \boldsymbol{r}, \boldsymbol{s}_m \rangle \Big\}. \quad (30)$$

b) Sub-optimal DCT based Receiver: The sub-optimal receiver configuration for $2M$-ary biU-FSK is presented in Fig. 8, which reduces the receiver complexity from $\mathcal{O}\left(M^2\right)$ for the optimal ML receiver to $\mathcal{O}\left(M\log_2(M)\right)$. The symbols $r[\overline{n}]$ for $\overline{n} = 0, 1, \cdots, 2M-1$ are obtained via analog to digital conversion of $r(t)$. Thereafter, the symbols of the biorthogonal dictionary, $\boldsymbol{\mathcal{D}}_{\mathrm{b}}$ are reconstructed from $r[\overline{n}]$ as:

$$\tilde{r}[n] = r[n] - r[M+n], \quad (31)$$

for $n = 0, 1, \cdots, M-1$, from which, $\boldsymbol{R}_{\tilde{m}}$ is obtained using M-order DCT as in (20). Subsequently, the transmitted waveform is identified using the frequency and polarity identification as in (21) and (22), respectively.

It may be speculated that the sub-optimal receiver may have better or comparable performance as that of the optimal receiver because of the use of orthogonal (or biorthogonal) symbols (after reconstruction) for frequency and polarization identification. However, this is incorrect because the sequential transmission of positive and negated negative samples increases the symbol duration to $2\tilde{T}_{\mathrm{s}}$. Thereby, symbol reconstruction (31) increases the noise variance by a factor of two (for the same symbol energy); which influences the performance. On the other hand, for the optimal ML receiver, the noise variance is curtailed due to matched filtering.

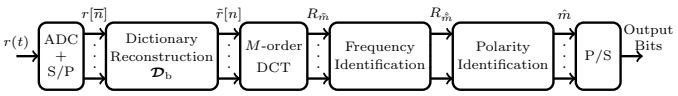

Fig. 8: Sub-optimal DCT based receiver structure for $2M$-ary biU-FSK.

TABLE I: Spectral efficiencies of the M-ary DC-FSK, $2M$-ary biDC-FSK, M-ary U-FSK, $2M$-ary biU-FSK and M-ary PPM in bit/s/Hz.

Modulation	η
M-ary DC-FSK	$\frac{2\log_2(M)}{M}$
$2M$-ary biDC-FSK	$\frac{2\log_2(2M)}{M}$
M-ary U-FSK	$\frac{\log_2(M)}{M}$
$2M$-ary biU-FSK	$\frac{\log_2(2M)}{M}$
M-ary PPM	$\frac{2\log_2(M)}{M}$

C. Spectral Efficiencies

The signal bandwidth for M-ary DC-FSK and M-ary U-FSK for sufficiently large M is approximately $B \approx M\Delta f = M/2T_{\mathrm{s}}$ (evaluated by neglecting the out-of-band energy on the harmonics of clipped waveform for M-ary U-FSK). Furthermore, the data-rate, R_{b} for M-ary DC-FSK and M-ary U-FSK is $\log_2(|\boldsymbol{\mathcal{D}}_{\perp}^{\mathrm{DC}}|)/T_{\mathrm{s}}$ and $\log_2(|\boldsymbol{\mathcal{D}}_{\perp}^{\mathrm{U}}|)/2T_{\mathrm{s}}$, respectively. Related spectral efficiencies are reported in Table I. By biorthogonal extension of M-ary DC-FSK and M-ary U-FSK to $2M$-ary biDC-FSK and $2M$-ary biU-FSK, the spectral efficiency is increased by $\frac{2}{M}$ and $\frac{1}{M}$, respectively. It is accentuated that biorthogonal extention of M-ary PPM is impossible. Hence, it manifests same spectral efficiency as that of M-ary DC-FSK. The spectral efficiency of M-ary PPM is evaluated considering that the pulse energy is located in bandwidth, $M/(2T_{\mathrm{s}})$. Though, this is an optimistic assumption for rectangular pulses with time width of $\Delta = T_{\mathrm{s}}/M$. Furthermore, the spectral efficiency considered for M-ary PAM in the subsequent sections corresponds to $\log_2(M)$ bit/s/Hz [14].

D. Distance Analysis Related to Energy

Fig. 9 provides a histogram of the squared normalized distances for the proposed approaches, i.e., $\overline{d}^2_{i,j} = d^2_{i,j}/2E^{(\cdot)}_{\mathrm{s}_{(\mathrm{elec})}}$, where $d^2_{i,j} = \|s_i(t) - s_j(t)\|^2 \ \forall i \neq j$. The simulations confirm the analytical findings in (16) and (29). Notably, if we consider $d^2_{i,j}$ with $|j-i| = M$ (for biorthogonal dictionary), the squared minimum Euclidean distance for $2M$-ary biDC-FSK is doubled compared to when $|j-i| \neq M$. Note that, the use of $2M$-ary biDC-FSK and $2M$-ary biU-FSK increases the spectral efficiency compared to M-ary DC-FSK and M-ary U-FSK, respectively, and also retains the same squared minimum Euclidean distance. Thus, it is anticipated that the BER performances of $2M$-ary biDC-FSK and $2M$-ary biU-FSK would be same as that of M-ary DC-FSK and M-ary U-FSK in AWGN for same symbol energy. Accordingly, we only analyse the performance of biorthogonal schemes, i.e., $2M$-ary biDC-FSK and $2M$-ary biU-FSK in previous and subsequent sections.

The average electrical and the optical powers for the trans-

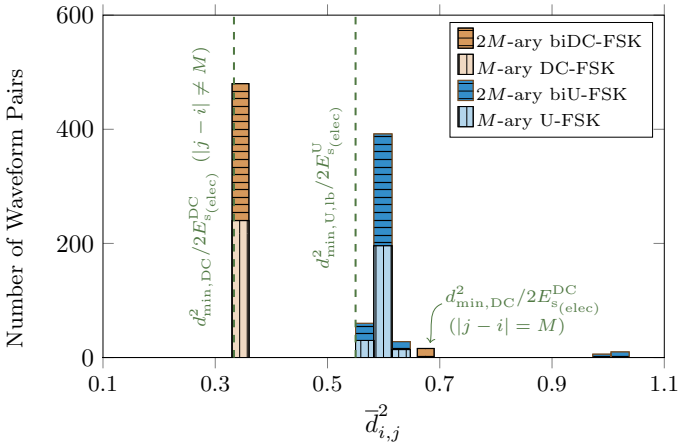

Fig. 9: Histogram of the squared normalized distances, i.e., $\bar{d}^2_{i,j} = d^2_{i,j}/2E^{(\cdot)}_{s_{(\mathrm{elec})}}$, where $d^2_{i,j} = \|s_i(t) - s_j(t)\|^2\ \forall i \neq j$ evaluated for M-ary DC-FSK, $2M$-ary biDC-FSK, M-ary U-FSK and $2M$-ary biU-FSK.

TABLE II: Average electrical power and optical powers of the waveforms for the proposed approaches. Here, $P_{(\mathrm{elec})} = E_{s_{(\mathrm{elec})}}/T_{\mathrm{s}}$ and $P_{(\mathrm{opt})} = E_{s_{(\mathrm{opt})}}/T_{\mathrm{s}}$ for both the approaches.

Modulation	$P_{(\mathrm{elec})}$	$P_{(\mathrm{opt})}$
$2M$-ary biDC-FSK	$\frac{A^2}{2} + \beta^2_{\mathrm{DC}}$	$\beta_{\mathrm{DC}} = A$
$2M$-ary biU-FSK	$\frac{A^2}{4}$	$\frac{A}{\pi}$

mit waveforms, given in Table II are evaluated using:

$$P_{(\mathrm{elec})} = \frac{1}{T_{\mathrm{s}}}\int_0^{T_{\mathrm{s}}} s_m(t)^2 \mathrm{d}t \quad \text{and} \quad P_{(\mathrm{opt})} = \frac{1}{T_{\mathrm{s}}}\int_0^{T_{\mathrm{s}}} s_m(t) \mathrm{d}t. \tag{32}$$

Using Table I, Table II and dropping the superscripts (specifying different approaches) from energy expressions, $E^{\mathrm{DC}}_{s_{(\mathrm{elec})}}$ and $E^{\mathrm{U}}_{s_{(\mathrm{elec})}}$, the electrical and optical SNR per bit at the receiver are specified as:

$$\frac{E_{b_{(\mathrm{elec})}}}{N_0} = \frac{P_{(\mathrm{elec})}}{\eta B N_0} \quad \text{and} \quad \frac{E_{b_{(\mathrm{opt})}}}{N_0} = \frac{P_{(\mathrm{opt})}}{\eta B N_0}. \tag{33}$$

Moreover, $P_{(\mathrm{elec})}$ and $P_{(\mathrm{opt})}$ are related to each other as:

$$\alpha_{\mathrm{EO}} = \frac{P_{(\mathrm{elec})}}{P_{(\mathrm{opt})}}, \tag{34}$$

where, α_{EO} represents the electrical-to-optical conversion efficiency. For any $E_{b_{(\mathrm{elec})}}/N_0$, $E_{b_{(\mathrm{opt})}}/N_0$ is achieved as $E_{b_{(\mathrm{opt})}}/N_0 = \alpha^{-1}_{\mathrm{EO}} E_{b_{(\mathrm{elec})}}/N_0$. α_{EO} specifies how much electrical power is converted to the optical power and is evaluated by scaling the optical power to unity, i.e., $P_{(\mathrm{opt})} = 1$ W as proposed by Armstrong and Schmidt in [28]. The normalization $P_{(\mathrm{opt})} = 1$ W implies a fair comparison relative to the average emitted optical power, but does not consider any constraint on the peak optical power limitation. Furthermore, such normalization leads to $A = \beta_{\mathrm{DC}} = 1$ for $2M$-ary biDC-FSK and $A = \pi$ for $2M$-ary biU-FSK resulting in α_{EO} equal to $3/2$ and $\pi^2/4$ for $2M$-ary biDC-FSK and $2M$-ary biU-FSK, respectively.

E. Complexity Analysis

For the proposed methods, the transmitter complexity is autonomous from M because LUTs are used. However, to generate LUT, M-order IDCT is implemented M times. Since M-order DCT/IDCT requires $2M\log_2(M) - M + 1$ arithmetic operations, the LUTs are generated utilizing $M\left[2M\log_2(M) - M + 1\right]$ arithmetic operations. The optimal receivers for M-ary DC-FSK and $2M$-ary biDC-FSK require M^2 and $2M^2$ arithmetic operations, respectively. For the low-complexity receiver for M-ary DC-FSK/$2M$-ary biDC-FSK, the receiver computational complexity is reduced to $2M\log_2(M) - M + 1$ arithmetic operations. The optimal receivers for M-ary U-FSK and $2M$-ary biU-FSK require $2M^2$ and $4M^2$ arithmetic operations. Whereas, for sub-optimal receiver, $2M\log_2(M) + 1$ arithmetic operations are needed.

IV. Receiver Design for Time Dispersive Channels

In Section III, we considered a simplified AWGN channel for receiver design. These receivers evaluate the inner product over a symbol duration of T_{s}. However, for a time dispersive channel, the intensity waveform is reflected/bounced multiple times before it reaches the receiver. Therefore, it is anticipated that, if the conventional receiver defined for AWGN is used for the time dispersive channel, BER performances will be degraded. Considering a channel impulse response vector, $\boldsymbol{h}$ and a delay spread of $\Delta\tau$, it is expected that the symbol duration of the received symbols would be $T_{\mathrm{s}} + \Delta\tau$. As shall be reported in the simulation section (Section V), the order of magnitude of the expected VLC application permits to assume that $T_{\mathrm{s}} \gg \Delta\tau$ and therefore, $\Delta\tau/T_{\mathrm{c}} \ll T_{\mathrm{s}}/T_{\mathrm{c}} = M_{\mathrm{c}}$. This consideration implies a weak inter-symbol interference (ISI). Furthermore, it may be possible that the received waveforms may suffer from local phase shift due to the channel. Therefore, hereby, we propose an improved receiver design which takes into account the temporal spreading of the received waveform and any phase shift that may occur. Like AWGN channel, in case of time dispersive channels with negligible ISI, the optimal receiver is based on ML criterion for both proposed approaches. The ML criterion is given as:

$$\hat{m} = \arg\min_m \|\boldsymbol{r} - \boldsymbol{h} \otimes \boldsymbol{s}_m\|^2. \tag{35}$$

The ML criterion (35) dictates to find the maximum value of real-valued cross-correlation between the received symbols, $\boldsymbol{r}$ and the respective dictionary symbols, i.e., $\tilde{\boldsymbol{s}}_m \in \boldsymbol{\mathcal{D}}_{\mathrm{b}}$ (used for $2M$-ary DC-FSK) or $\boldsymbol{s}_m \in \boldsymbol{\mathcal{D}}^{\mathrm{U}}_{\mathrm{b}}$ (for $2M$-ary biU-FSK) convolved with the channel impulse response vector, $\boldsymbol{h}$. Thus, considering $m \in \{0, 1, \cdots, 2M-1\}$, the ML receiver is implemented as:

$$\hat{m} = \arg\max_m \left\{ \langle \boldsymbol{r}, \boldsymbol{h} \otimes \tilde{\boldsymbol{s}}_m \rangle - \frac{1}{2}\|\boldsymbol{h} \otimes \tilde{\boldsymbol{s}}_m\|^2 \right\}, \tag{36}$$

for $2M$-ary DC-FSK and

$$\hat{m} = \arg\max_m \left\{ \langle \boldsymbol{r}, \boldsymbol{h} \otimes \boldsymbol{s}_m \rangle - \frac{1}{2}\|\boldsymbol{h} \otimes \boldsymbol{s}_m\|^2 \right\}, \tag{37}$$

for $2M$-ary U-FSK. The impact of channel impulse response on each frequency tone is different resulting in different power

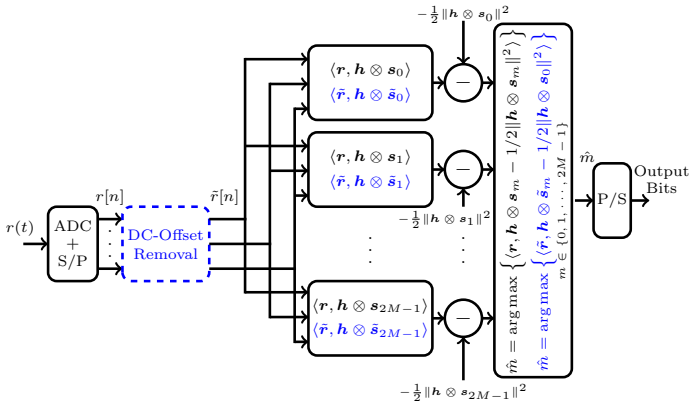

Fig. 10: Improved receiver configurations for $2M$-ary biDC-FSK and $2M$-ary biU-FSK for time dispersive channels. In addition to the operations in black color, the operations performed in blue color corresponds to $2M$-ary biDC-FSK receiver. All the operations in black corresponds to what is needed for the ML receiver of $2M$-ary biU-FSK.

profiles for the received symbols. Therefore, (36) and (37) take into account the energy of each symbol after channel transmission and evaluates the inner product over the extended symbol duration $T_{\rm s} + \Delta\tau$. Thus, any local phase shift that may occur will be taken into account directly. The system configuration of improved receiver for time dispersive channels is given in Fig. 10. In practical scenario, $\boldsymbol{h}$ should be known apriori to implement this receiver.

V. Performance Analysis

In this section, an overview of the performances is provided for the proposed approaches. We appraise the following performance parameters: (i) BER in AWGN as a function of electrical and optical SNR per bit; (ii) energy efficiency with respect to spectral efficiency considering an AWGN channel; (iii) the impact of PMOPR on optical power in an AWGN channel; (iv) impact of time dispersive channel on the waveforms; and (v) the energy efficiency performance versus data rate, $R_{\rm b}$ in a time dispersive channel. The simulation parameters are outlined in Table III.

A. Performance over AWGN Channel

1) Bit Error Rate Performance: Fig. 11 depicts the BER performance of the optimal and the sub-optimal receiver for M-ary U-FSK over an AWGN channel. As expected, the optimal ML receiver is better than the sub-optimal one by less than 1 dB. Therefore, subsequent simulations only consider the optimal ML receiver. Furthermore, the BER performances of $2M$-ary biDC-FSK and $2M$-ary biU-FSK as a function of $E_{\rm b_{(elec)}}/N_0$ and $E_{\rm b_{(opt)}}/N_0$ are illustrated in Fig. 12 and Fig. 13, respectively. OOK and M-ary PAM are provided as references. Fig. 13 is obtained considering $P_{\rm (opt)} = 1$ W. Both Fig. 12 and Fig. 13 indicate that $2M$-ary biU-FSK manifests superior BER performance compared to $2M$-ary biDC-FSK. The BER performance of $2M$-ary biDC-FSK is negatively affected because of the DC-offset; which increases the energy requirements. On the other hand, the required $E_{\rm b_{(elec)}}/N_0$ and $E_{\rm b_{(opt)}}/N_0$ to achieve a given BER for M-ary PAM increase with an increase in alphabet cardinality, M. This

TABLE III: Simulation parameters to evaluate the performance of $2M$-ary biDC-FSK and $2M$-ary biU-FSK.

Parameter	Values
Channel	AWGN, i.e., $h(t) = \delta(t)$
	(Fig. 11, 12, 13, 14, 15, 16)
	Ceiling Bounce Model
	(Fig. 17, 18, 19)
Number of Chips	M for $2M$-ary biDC-FSK
	$2M$ for $2M$-ary biU-FSK
$P_{\rm (opt)}$	1 W (Fig. 13,15)
$P_{\rm (opt)}^{\rm (peak)}$	$\max\{\lvert s_m(t)\rvert\}$ (Fig. 16)
$R_{\rm b}$	$1{\rm kbps} - 10{\rm Mbps}$
	(Fig. 17, 18, 19)
Delay Spread, $\Delta\tau$	10 ns
	(Fig. 17, 18, 19)
Speed of Light, c	3×10^8 m/s
Optical Path Loss, ζ	1
Monte Carlo Runs	10^6

completely contradicts the behavior of $2M$-ary biDC-FSK and $2M$-ary biU-FSK, for which, the required $E_{\rm b_{(elec)}}/N_0$ and $E_{\rm b_{(opt)}}/N_0$ decrease with an increase in alphabet cardinality. The difference in energy requirements for $2M$-ary biDC-FSK and $2M$-ary biU-FSK is compliant with the analytical analysis in Section III. Indeed, it is expected from (17) and (29), that for $2M$-ary biDC-FSK, the required electrical energy is approximately $10\log_{10}\left(\gamma^{\rm U}/\gamma^{\rm DC}\right) \approx 2.2$ dB higher than the electrical energy requirement for $2M$-ary biU-FSK which is confirmed by simulation results in Fig. 12. Furthermore, in terms of $E_{\rm b_{(opt)}}/N_0$ (Fig. 13), the performance of $2M$-ary biU-FSK is markedly (approximately 4 dB) better than $2M$-ary biDC-FSK because $\alpha_{\rm EO}$ is smaller for $2M$-ary biDC-FSK due to the adoption of DC-offset, which is compliant with the analytical results as $\alpha_{\rm EO}$ (34) corresponds to $3/2$ for $2M$-ary biDC-FSK versus $\pi^2/4$ for $2M$-ary biU-FSK.

2) Energy Efficiency versus Spectral Efficiency: Fig. 14 and Fig. 15 demonstrate the evolution of required $E_{\rm b_{(elec)}}/N_0$ and $E_{\rm b_{(opt)}}/N_0$ with respect to η for a BER of 10^{-3}. In Fig. 14, Shannon's fundamental limit (given by (12)) is presented to identify the pessimistic lower bound on $E_{\rm b_{(elec)}}/N_0$ that can be realized for a given spectral efficiency, η. Theoretically, communication is possible at points below the Shannon's fundamental limit curve and impossible at points above it. Futhermore, the aim is to be as close as possible to the asymptotic limit of -1.59 dB. It is shown that $2M$-ary biU-FSK exhibits better performance compared to $2M$-ary biDC-FSK in terms of required $E_{\rm b_{(elec)}}/N_0$ and $E_{\rm b_{(opt)}}/N_0$ over a range of modulation alphabet cardinalities. In terms of $E_{\rm b_{(elec)}}/N_0$, the performance approaches Shannon's fundamental limit for an exceedingly large M. Large values of M signifies a radical reduction in spectral efficiency, η, but that can be compatible with the targeted low data applications for

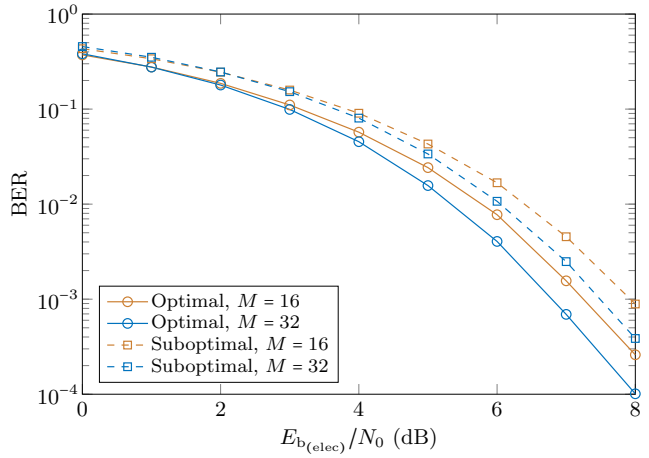

Fig. 11: Simulated BER performance comparison for the optimal and the sub-optimal receiver of M-ary U-FSK. It is highlighted that these receiver configurations can also be employed for $2M$-ary biU-FSK.

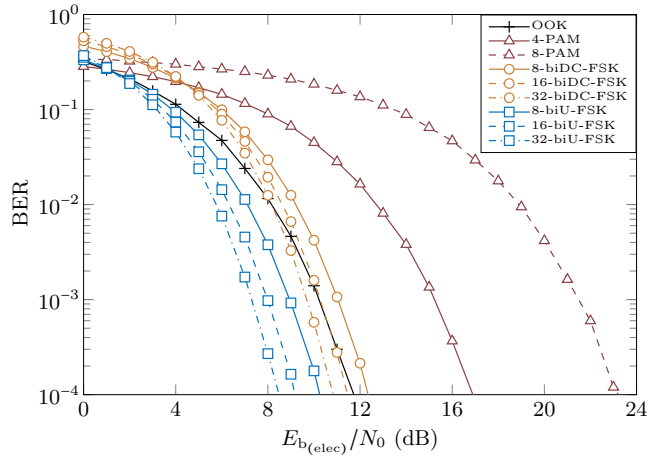

Fig. 12: Simulated BER vs $E_{b_{(elec)}}/N_0$ comparison between $2M$-ary biDC-FSK and $2M$-ary biU-FSK.

IoT. On the other hand, Fig. 14 and Fig. 15 also signify that the required $E_{b_{(elec)}}/N_0$ and $E_{b_{(opt)}}/N_0$ increase with an increase in alphabet cardinality, M for M-ary PAM modulations. It is accentuated that the gap between the (pessimistic) Shannon's fundamental limit and the $E_{b_{(elec)}}/N_0$ is common as demonstrated in [10], [27] and [29]. However, this gap can be reduced by using appropriate channel coding techniques [11], [12].

3) Impact of Peak-to-Mean Optical Power Ratio on Optical Power Efficiency: In practical scenarios, PMOPR conjugated with the DAC dynamic range limitation may induce significant performance limitations. In that case, it is relevant to limit the peak optical power to a fixed value (unity) instead of fixing the average optical power to unity. To appraise this, we introduce peak optical power, $P^{\text{peak}}_{(\text{opt})}$, which is linked to $P_{(\text{opt})}$ as:

$$P^{\text{peak}}_{(\text{opt})} = \max\left\{|s_m(t)|\right\} = \lambda_{(\text{opt})} P_{(\text{opt})}. \tag{38}$$

$\lambda_{(\text{opt})}$ is PMOPR whose value equal to 2, π and M for $2M$-ary biDC-FSK, $2M$-ary biU-FSK and M-ary PPM, respectively considering an optical power equal to unity (1 W). Fig. 16 illustrates the BER performances of the proposed techniques as a function of $E^{\text{peak}}_{b_{(opt)}}/N_0$, where $E^{\text{peak}}_{b_{(opt)}}/N_0 = \lambda_{(\text{opt})} E_{b_{(opt)}}/N_0$. DRL in the legend attributes to *dynamic range limitation*; which indicates unit peak optical power for the signal. From Fig. 16, it is obvious that by including the limited dynamic range, a significant penalty is brought about on PPM's performance compared to when no dynamic range limitation is included, i.e, $P_{(\text{opt})} = 1$ W. It also penalizes $2M$-ary biU-FSK, but lesser than M-ary PPM. $2M$-ary biDC-FSK embodies approximately the same performance regardless of dynamic range limitation because it exhibits the lowest

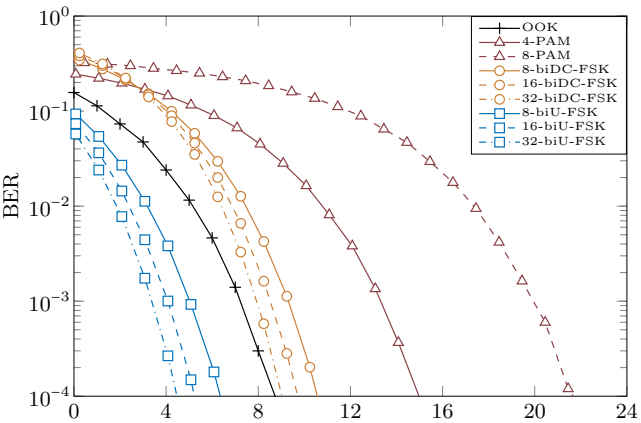

Fig. 13: Simulated BER vs $E_{b_{(opt)}}/N_0$ comparison between $2M$-ary biDC-FSK and $2M$-ary biU-FSK.

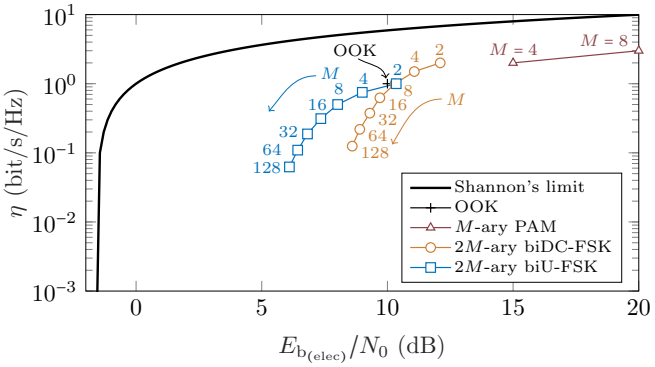

Fig. 14: The evolution of required $E_{b_{(elec)}}/N_0$ with respect to η to achieve a BER of 10^{-3}. The alphabet cardinalities presented in the figure correspond to $2M$ for the proposed approaches.

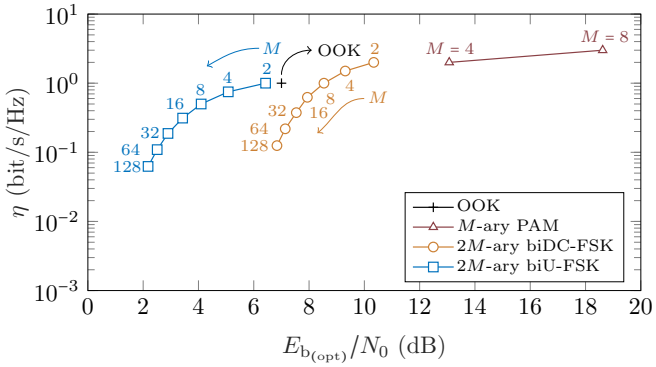

Fig. 15: The evolution of required $E_{b_{(opt)}}/N_0$ with respect to η to achieve a BER of 10^{-3}. The alphabet cardinalities presented in the figure correspond to $2M$ for the proposed approaches.

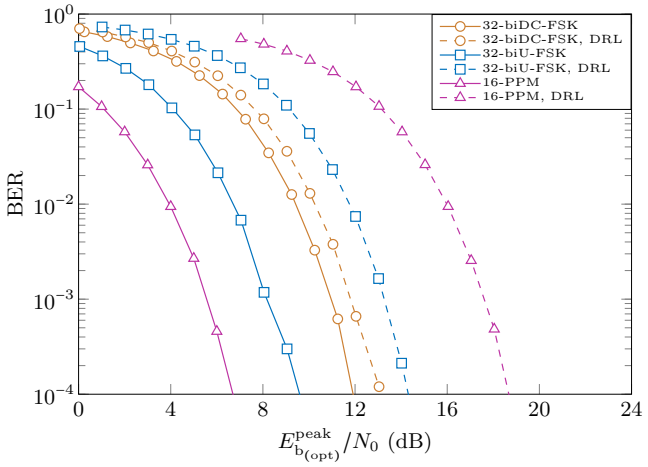

Fig. 16: BER vs $E^{\text{peak}}_{\text{b(opt)}}/N_0$ comparison between $2M$-ary biDC-FSK, $2M$-ary biU-FSK and M-ary PPM.

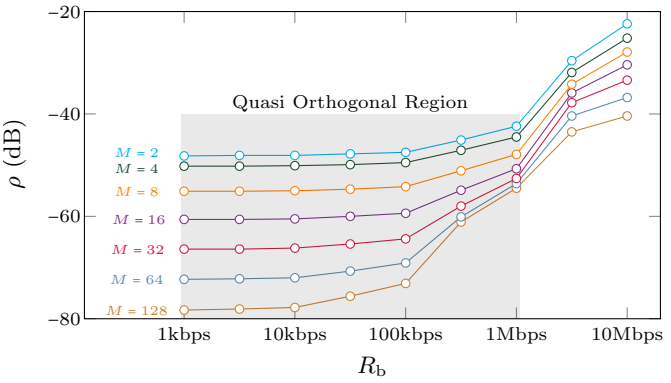

Fig. 17: Impact of channel reflections on the orthogonality of $\boldsymbol{\mathcal{D}}_{\perp}$ as a function of data rate, R_{b}.

PMOPR.

B. Performance over Time Dispersive VLC Channel

In this subsection, we measure the impact of the channel reflections on required $E_{\text{b(elec)}}/N_0$ using receivers proposed for AWGN channel (Section III) and improved receiver for time dispersive VLC channel (Section IV). Before presenting the results, we shall first introduce a typical time dispersive VLC channel model and analyse possible impacts in terms of ISI, frequency selectivity, and orthogonality (for $\boldsymbol{\mathcal{D}}_{\perp}$).

1) Channel Model: We consider ceiling bounce model proposed by Carruthers and Kahn [30] to simulate the impulse response of time dispersive VLC channel, $h(t)$. Considering that the transmitter and the receiver are located in planes parallel to the floor and are directed towards the ceiling, the model provides closed-form expressions to obtain $h(t)$. Essentially, $h(t)$ is defined via the optical path loss, ζ; and the root-mean-square (rms) delay spread, $\Delta\tau$ of the channel as [30]:

$$h(t) = \zeta \frac{6\alpha^2}{(t+\alpha)^7} u(t), \tag{39}$$

where $u(t)$ is the unit step function. The optical path loss, ζ is normalized to 1, $\alpha = 2H/c$, where H is the height of the room ceiling from the transmitter and the receiver and c is the speed of light. α is linked to $\Delta\tau$ as:

$$\Delta\tau = \frac{\alpha}{12}\sqrt{\frac{13}{11}}. \tag{40}$$

2) Impact of Time Disperive Channel on Waveforms: For typical indoor VLC scenarios, $\Delta\tau$ is approximately 10 ns [31], [32], which culminates in a coherence bandwidth, $B_{\text{coh}} = 1/\Delta\tau$ of approximately 100 MHz. Considering these channel characteristics with $M \geq 2$ for our proposed techniques and low data rate assumption of $R_{\text{b}} \leq 1$ Mbps, we infer the following:

- *weak ISI:* $\Delta\tau \ll T_{\text{s}}$ implies that $\Delta\tau/T_{\text{c}} \ll T_{\text{s}}/T_{\text{c}} = M_{\text{c}}$. Indeed, considering $T_{\text{s}} = \log_2(2M)/R_{\text{b}}$, and the worst case scenario of $M = 2$ and $R_{\text{b}} = 1$ Mbps, the ratio $\Delta\tau/T_{\text{s}}$ is as low as 5×10^{-3}. This assumption is consolidated for large M since $T_{\text{s}} = \log_2(M)/R_{\text{b}}$. The symbol portion impacted by the ISI, quantified via $\Delta\tau/T_{\text{s}}$, decreases. Consequently, we would have weak ISI and also expect weak inter-carrier-interference (ICI) which shall be verified subsequently.
- *weak local frequency selectivity:* $2\Delta f$, i.e., the bandwidth of main lobe of a tone is small compared to B_{coh}, i.e., $2\Delta f \ll B_{\text{coh}}$. As an example, consider $R_{\text{b}} = 1$ Mbps for the worst case scenario of $M = 2$. In this case, $2\Delta f \approx 0.5$ Mbps, which is far less than $B_{\text{coh}} = 100$ MHz. This means that different waveforms will approximately conserve their shapes since they are only attenuated and phase shifted. We can then foresee that the distance between waveforms is mainly preserved (meaning preservation of orthogonality for $\boldsymbol{\mathcal{D}}_{\perp}$), which is evaluated hereafter.
- *weak loss of orthogonality leading to weak intercarrier interferences (ICI):* The proposed techniques not orthogonal modulations (see Section III), however, their dictionaries, $\boldsymbol{\mathcal{D}}^{\text{DC}}_{\text{b}}$ and $\boldsymbol{\mathcal{D}}^{\text{U}}_{\text{b}}$ are generated from an orthogonal dictionary $\boldsymbol{\mathcal{D}}_{\perp}$ of the (bipolar) FSK waveforms. Therefore, we analyse the impact of time dispersive channel on orthogonality considering $\boldsymbol{\mathcal{D}}_{\perp}$. To quantify the orthogonality loss leading to ICI and possible wrong frequency identification at receiver, we evaluate mean normalized correlation coefficient, ρ, between different tones after transmission via time dispersive channel. Ideally, for orthogonal symbols, $\rho = 0$. ρ, for transmitted orthogonal symbols from $\boldsymbol{\mathcal{D}}_{\perp}$ through the time dispersive channel, is defined as:

$$\rho = \frac{1}{M}\sum_{i=1}^{M}\left(\frac{1}{M-1}\sum_{\substack{j=1\\ j\neq i}}^{M}\frac{\langle \boldsymbol{h}\otimes\tilde{\boldsymbol{s}}_i, \boldsymbol{h}\otimes\tilde{\boldsymbol{s}}_j\rangle}{\|\boldsymbol{h}\otimes\tilde{\boldsymbol{s}}_i\|^2}\right). \tag{41}$$

ρ on the dB scale against R_{b} is illustrated in Fig. 17. It reveals that the loss of orthogonality is extremely weak even for $R_{\text{b}} = 10$ Mbps. Though the correlation computation has been done for $\boldsymbol{\mathcal{D}}_{\perp}$, it can be expected that the ICI incorporated due to channel reflections may not affect the performance of the FSK based proposed techniques. However, some additional ICI is anticipated due to unipolar conversion of the transmit symbols and

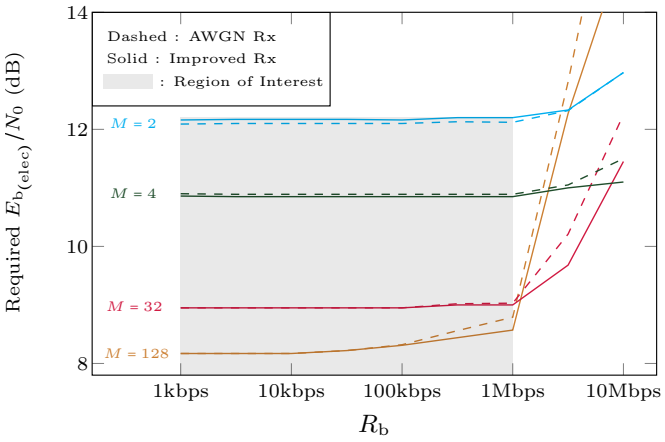

Fig. 18: Required $E_{b_{(elec)}}/N_0$ for $2M$-ary biDC-FSK to achieve a BER of 10^{-3} as a function of data rate, R_b considering ceiling bounce model.

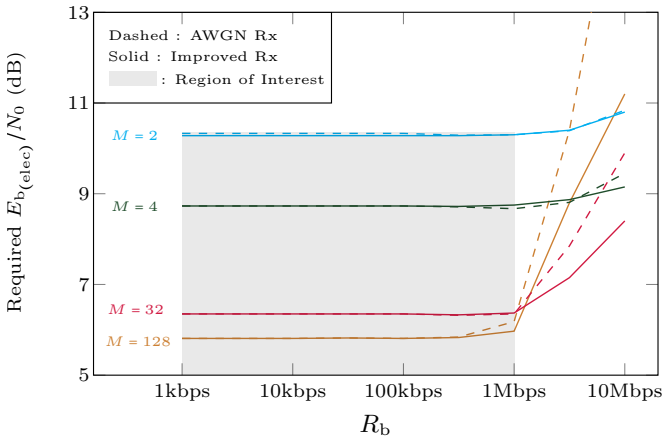

Fig. 19: Required $E_{b_{(elec)}}/N_0$ for $2M$-ary biU-FSK to achieve a BER of 10^{-3} as a function of data rate, R_b considering ceiling bounce model.

the impact of time dispersive channel on the transmit symbols.

3) Performance and Energy Efficiency versus Data Rate: Fig. 18 and Fig. 19 portray the required $E_{b_{(elec)}}/N_0$ needed to achieve a BER of 10^{-3} as a function of data rate, R_b. We consider ceiling bounce model with $\Delta\tau = 10$ ns. The performances of AWGN receiver presented in Section III and improved receiver design for dispersive channels (Section IV) are compared. Up to 1 Mpbs the performances of both receivers are similar. However, for $R_b > 1$ Mbps, the performance of improved receivers are better compared to the AWGN as they also take into account phase shift that may affect frequency tones due to time dispersive channels. Since we target low data rate applications, therefore, we confine the region of interest (ROI) up to 1 Mbps. In the ROI, as both receivers have similar performances, it may be better to use the AWGN receiver because channel estimation to make decisions on the transmitted frequencies is not needed. Furthermore, for $R_b > 1$ Mpbs, there is a drastic increase in required $E_{b_{(elec)}}/N_0$ for large M. This is because even if local flat frequency selectivity is reinforced (see Section V-B2), the drawback is that the gain and phase affecting the frequency tones is not the same in the global bandwidth, B, i.e., which corresponds to wideband frequency selectivity phenomenon. Indeed, we recall that $B = (R_b M)/\log_2(2M)$, therefore, when M increases to infinity, then the condition $B \ll B_{coh}$ is not true anymore. Contrary to that, for lower alphabet cardinalities, M, the increase in required $E_{b_{(elec)}}/N_0$ for $R_b > 1$ Mpbs is less because the response of the channel is relatively flat in the global signal bandwidth, B (e.g., $M = 2$ and $R_b \leq 10$ MHz implies $B/B_{coh} \leq 0.1$). Anyway, the required $E_{b_{(elec)}}/N_0$ remains less for the approaches with higher M according to global analysis.

VI. Conclusions

We propose two variants of M-ary FSK for IoT connectivity using VLC. These techniques can outperform M-ary PPM due to their inherent lower PMOPR. Moreover, the proposed techniques are more energy efficient in terms of both electrical and optical powers compared to linear modulations, such as OOK and M-ary PAM. For example, 256-ary biU-FSK permits an energy economy of more than 4 dB compared to OOK. Furthermore, it can be observed that the performances of the proposed approaches in multipath VLC channels are almost the same as in AWGN because of weak ISI impact and flat frequency fading for low data rate IoT communications (< 1 Mbps). The practicality of these approaches is enhanced by the fact that the low-complexity receivers of the proposed approaches can be applied to DCT/IDCT based FOFDM approaches available in the literature to provide both low data rate/high data rate communication modes. A logical extension of this work could be to investigate on low complexity channel coding to boost the performance of these approaches.

References

[1] D. Karunatilaka, F. Zafar, V. Kalavally, and R. Parthiban. LED based indoor visible light communications: State of the art. *IEEE Commun. Surv. Tut.*, 17(3):1649–1678, 2015.

[2] S. Schmid, B. von Deschwanden, S. Mangold, and T. R. Gross. Adaptive software-defined visible light communication networks. *IEEE/ACM Intl. Conf. on Internet-of-Things Design and Implementation*, pages 109–120, 2017.

[3] E. R. Vercellone, V. Ferrandiz, J. Aubert, and M. Gasulla. Using LEDs for visible light communication and as a wake-up mechanism in the internet of things. *ACM Conf. on Embedded Network Sensor Systems*, page 49, 2017.

[4] M. Jarzyna and K. Banaszek. Efficiency of optimized pulse position modulation with noisy direct detection. In *IEEE Intl. Conf. on Space Optical Systems and Applications*, pages 166–171, 2017.

[5] M. S. Islim and H. Haas. Modulation techniques for Li-Fi. *ZTE communications*, 14(2):29–40, 2016.

[6] A. Pradana, N. Ahmadi, T. Adiono, W. A. Cahyadi, and Y.-H. Chung. VLC physical layer design based on pulse position modulation (PPM) for stable illumination. In *Intl. Symposium on Intelligent Signal Processing and Communication Systems*, pages 368–373. IEEE, 2015.

[7] A. Chizari, M. V. Jamali, S. Abdollahramezani, J. A. Salehi, and A. Dargahi. Visible light for communication, indoor positioning, and dimmable illumination: A system design based on overlapping pulse position modulation. *Optik*, 151:110–122, 2017.

[8] A. Nuwanpriya, S.-W. Ho, J. A. Zhang, A. J. Grant, and L. Luo. PAM-SCFDE for optical wireless communications. *J. Lightw. Tech.*, 33(14):2938–2949, 2015.

[9] C. E. Shannon. A mathematical theory of communication. *Bell Sys. J.*, 27(3):379–423, 1948.

[10] K. Kikuchi and M. Osaki. Highly-sensitive coherent optical detection of m-ary frequency-shift keying signal. *Opt. Express*, 19(26):B32–B39, 2011.

[11] Y. Roth, J.-B. Doré, L. Ros, and V. Berg. Turbo-FSK, a physical layer for low-power wide-area networks: Analysis and optimization. *Comptes Rendus Physique*, 18(2):178–188, 2017.

[12] Y. Roth, J.-B. Doré, L. Ros, and V. Berg. The physical layer of low power wide area networks: Strategies, information theory's limit and existing solutions. *Chapter 7, Advances in Signal Processing: Reviews, Book Series*, 1, 2018.

[13] H Park and J. R. Barry. Trellis-coded multiple-pulse-position modulation for wireless infrared communications. *IEEE Trans. Commun.*, 52(4):643–651, 2004.

[14] Z. Ghassemlooy, W. Popoola, and S. Rajbhandari. *Optical wireless communications: system and channel modelling with MATLAB®*. CRC press, 2012.

[15] S. Arnon. The effect of clock jitter in visible light communication applications. *J. Light. Tech.*, 30(21):3434–3439, 2012.

[16] H.-J. Jang, J.-H. Choi, Z. Ghassemlooy, and C. G. Lee. PWM-based PPM format for dimming control in visible light communication system. In *Intl. Symp. Commun. Sys., Net. Dig. Sig. Process*, pages 1–5. IEEE, 2012.

[17] S. He, G. Ren, Z. Zhong, and Y. Zhao. M-ary variable period modulation for indoor visible light communication system. *IEEE Commun. Lett.*, 17(7):1325–1328, 2013.

[18] G. M. M. Yamga, A. R. Ndjiongue, and K. Ouahada. Low complexity clipped frequency shift keying (FSK) for visible light communications. *Intl. Conf. on Adaptive Science & Technology*, pages 1–6, 2018.

[19] J. Zhou, Y. Qiao, T. Zhang, E. Sun, M. Guo, Z. Zhang, X. Tang, and F. Xu. FOFDM based on discrete cosine transform for intensity-modulated and direct-detected systems. *J. Lightw. Techn.*, 34(16):3717–3725, 2016.

[20] K. R. Rao and P. Yip. *Discrete cosine transform: algorithms, advantages, applications*. Academic press, 2014.

[21] N. Ahmed, T. Natarajan, and K. R. Rao. Discrete cosine transform. *IEEE Trans. Computers*, 100(1):90–93, 1974.

[22] A. W. Azim, Y. Le Guennec, and G. Maury. Decision-directed iterative methods for PAPR reduction in optical wireless OFDM systems. *Opt. Commun.*, 389:318–330, 2017.

[23] A. Weiss, A. Yeredor, and M. Shtaif. Iterative symbol recovery for power-efficient dc-biased optical OFDM systems. *J. Lightw. Tech.*, 34(9):2331–2338, 2016.

[24] H. Elgala, R. Mesleh, and H. Haas. Non-linearity effects and predistortion in optical ofdm wireless transmission using leds. *Intl. J. of Ultra Wideband Commun. Syst.*, 1(2):143–150, 2009.

[25] D. Tsonev, S. Videv, and H. Haas. Light fidelity (Li-Fi): towards all-optical networking. In *Broadband Access Communication Technologies VIII*, volume 9007, page 900702. International Society for Optics and Photonics, 2014.

[26] S. Dimitrov and H. Haas. *Principles of LED light communications: towards networked Li-Fi*. Cambridge University Press, 2015.

[27] J. G. Proakis and M. Salehi. *Digital communications*. McGraw-Hill, 2008.

[28] S. D. Dissanayake and J. Armstrong. Comparison of ACO-OFDM, DCO-OFDM and ADO-OFDM in IM/DD systems. *J. Lightw. Techn.*, 31(7):1063–1072, 2013.

[29] A. D. Ellis, J. Zhao, and D. Cotter. Approaching the non-linear Shannon limit. *J. Lightw. Tech.*, 28(4):423–433, 2009.

[30] J. B. Carruthers and J. M. Kahn. Modeling of nondirected wireless infrared channels. *IEEE Trans. Commun.*, 45(10):1260–1268, 1997.

[31] K. Lee, H. Park, and J. R. Barry. Indoor channel characteristics for visible light communications. *IEEE Commun. Lett.*, 15(2):217–219, 2011.

[32] M. Uysal, F. Miramirkhani, O. Narmanlioglu, T. Baykas, and E. Panayirci. Ieee 802.15. 7r1 reference channel models for visible light communications. *IEEE Commun. Mag.*, 55(1):212–217, 2017.